Twofold expansion of Indo-Pacific warm pool warps MJO lifecycle

M K Roxy[1,2*], **Panini Dasgupta**[1,3], **Michael J. McPhaden**[2], **Tamaki Suematsu**[4], **Chidong Zhang**[2] and **Daehyun Kim**[5]

[1]*Centre for Climate Change Research, Indian Institute of Tropical Meteorology, Pune 411008, India*

[2]*Pacific Marine Environmental Laboratory, National Oceanic and Atmospheric Administration, Seattle, Washington 98115, USA*

[3]*Department of Meteorology and Oceanography, College of Science and Technology, Andhra University, Visakhapatnam, Andhra Pradesh 530003, India*

[4]*Atmosphere and Ocean Research Institute, The University of Tokyo, Kashiwa 227-8654, Chiba, Japan*

[5]*Department of Atmospheric Sciences, University of Washington, Seattle, Washington 98195, USA*

Nature, submitted on 21 May 2019, revised on 26 July 2019 and on 02 September 2019

---

*Corresponding author address: Roxy Mathew Koll, Indian Institute of Tropical Meteorology, Pune 411008, India. E-mail: roxy@tropmet.res.in

Abstract

The Madden Julian Oscillation (MJO) is the most dominant mode of subseasonal variability in the tropics, characterized by an eastward moving disturbance of rain clouds. The MJO modulates the El Niño Southern Oscillation[1], tropical cyclones[2,3] and the monsoons[4-10]—and contributes to severe weather events over Asia, Australia, Africa, Europe and the Americas. MJO events travel a stretch of 12,000–20,000 kms over the tropical oceans, which has been warming during the twentieth and early-twenty first centuries in response to greenhouse gas forcing[11], and is projected to warm further. However, the impact of this warming on the MJO lifecycle is largely unknown. Here we show that rapid warming over the tropical oceans during 1981–2018 has warped the MJO lifecycle, with its residence time decreasing over the Indian Ocean by 3–4 days, and increasing over the Indo-Pacific Maritime Continent by 5–6 days. We find that these changes in the MJO lifecycle is associated with a twofold expansion of the Indo-Pacific warm pool, which has been expanding on an average by 2.3 $\times 10^5$ km^2 (the size of Washington State) per year during 1900–2018 and at an accelerated average rate of 4×10^5 km^2 (the size of California) per year during 1981–2018. The changes in the warm pool and the MJO are related to an increased rainfall over Southeast Asia, northern Australia, Southwest Africa and the Amazon, and drying over the west coast of United States and Ecuador.

Article

Each year, weather variability at subseasonal to seasonal timescales costs the global economy over $2 trillion, with $700 billion alone in the US (3.4% of US GDP in 2018)[12,13]. The Madden Julian Oscillation (MJO) contributes to more than 55% of this weather variability over the tropics[14]—and modulates the Asian[4,5], Australian[6] , African[7] and American monsoons[8-10], tropical cyclogenesis[2,3] and the El Niño Southern Oscillation (ENSO)[1]. The phase and strength of the MJO at a given location can enhance or suppress the tropical rainfall variability, modulating or triggering extreme weather events including hurricanes, droughts, flooding, heat waves and cold surges[15]. The MJO can also lead to dramatic impacts in mid-latitudes, and is a strong contributor to extreme events in the United States and Europe[16,17]. The intensity and propagation of the MJO is shown to influence the circulation pattern in the Arctic stratosphere and the polar vortex[18], emphasizing the far-reaching impact of MJO on the earth's climate system.

The MJO is an ocean-atmosphere coupled phenomenon, characterized by eastward moving disturbances of clouds, rainfall, winds, and pressure along the equator. It is the most dominant mode of the subseasonal variability in the tropics[19]. Using observations and model simulations, previous studies have attempted to understand the changes in the MJO in a warming climate[20]. They found a link between increasing carbon emission and changes in the intensity, frequency and propagation of the MJO over the last few decades of the twentieth century[20,21], though there is considerable uncertainty in the extent of the changes and the mechanisms involved. A statistical reconstruction of the MJO activity over 1905–2008 using tropical surface pressures shows a 13% increase per century in the MJO amplitude[22]. The reconstructed MJO activity agrees with the satellite-observed (since 1979) MJO variability on decadal timescales—but the trends disagree after 1997[23], which adds to the considerable uncertainty as to their magnitude. Studies also suggest an increasing trend in the MJO frequency after the mid-1970s[24,25], which has been linked to the long term warming in the tropical oceans[26]. Numerical model experiments under idealized global warming scenarios indicate that increasing the surface temperatures over the tropical oceans results in an organized MJO activity with a faster eastward propagation[21,27], though an understanding based on observations is pending.

Typically, the MJO events are initiated over the Indian Ocean and move eastward over the Maritime Continent to the Pacific (Extended Data Figure 1). Some of these events weaken or breakdown over the Maritime Continent or the central Pacific[28], but others propagate further to the east Pacific and occasionally continue into the Atlantic[29]. On average, MJO events travel a zonal distance of 12,000–20,000 kms (7,500–12,500 miles) over the generally warm tropical oceans. This entire stretch of the tropical ocean has been warming during the twentieth and early-twenty first centuries in response to greenhouse gas forcing[11], and is projected to warm further in the future. The rapid warming across the tropical basins is not uniform. In the equatorial belt, the largest warming during November–April when the MJO is active is observed over the Indo-Pacific warm pool (Figure 1). This warm pool is the largest region of permanently warm sea surface temperatures (SSTs > 28°C), covering an area greater than 2.7×10^7 km^2 (see the Methods section), over which there is vigorous deep convection. The tropical ocean warming has led to an expansion of this warm pool, particularly in the recent decades. Even though we have a preliminary understanding of the general changes in MJO amplitude and frequency in a warming climate, we do not know how the non-uniform ocean warming associated with the expanding warm pool may affect the MJO regionally.

In our study, we find a twofold expansion of the Indo-Pacific warm pool during 1981–2018, in comparison to 1900–1980, with the largest warming over the western Pacific. We show that this warm pool expansion has led to significant changes in the lifecycle of MJO events over the Indo-Pacific region. While the total period of the MJO does not show any detectable trends, its residence time (MJO phase duration) over the Indian Ocean has been reduced by 3–4 days while that over the Maritime Continent has increased by 5–6 days. Essentially, this means that MJO-related convective activity has grown shorter over the Indian Ocean while the convection over the Maritime Continent is being prolonged.

Results

Observed changes in MJO lifecycle

We select the MJO events which exhibit 1) strong coupling between tropical convection and largescale circulation, 2) prominent active eastward propagation and 3) an amplitude of the Real-time Multivariate (RMM) MJO index[30] that is greater than one for November–April, 1981–2018 (see the Methods section). From its normal initiation in the Indian Ocean (RMM Phase 1), the MJO propagates into the Central Pacific and beyond (Phase 8) in about 30–60 days (Extended Data Figure 2). We compute the average number of days of the selected MJO in each RMM phase to describe the MJO phase duration over the tropical ocean basins. In the RMM index, interannual variations, including those associated with ENSO[30], have been removed. This makes it suitable for our investigation focusing on the changes in the MJO related to global warming.

Figure 2 shows the timeseries of the MJO phase duration and how it has changed over time. The average period of the MJO does not exhibit any detectable trends and broadly remains within the normal 30–60 days' timescale (Extended Data Figure 2). However, a closer inspection (Figure 2) shows significant changes in individual phases, which essentially are offset while averaging over the entire MJO domain. Over the Indian Ocean (RMM phases 1, 2 and 3), the MJO phase duration decreases by 3–4 days, from an average of 19 days (during 1981–1999) to 15.4 days (during 2000–2018) (Figure 2a, b). Over the Maritime Continent and the west Pacific (RMM phases 5, 6 and 7), the MJO phase duration increases by 5–6 days, from an average of 17.5 days to 23 days (Figure 2c, d). The observed trends are statistically significant at the 95% confidence level. The changes are consistent with those documented by previous studies which compared the MJO activity across different RMM phases, using observations and climate model experiments[31,32]. This means that during recent decades, convective cloud bands associated with the MJO linger over the Indian Ocean for a shorter period, while they persist longer over the Maritime Continent and the west Pacific.

The role of Indo-Pacific warming

SST variations mediate the exchange of heat across the air-sea interface. High SSTs over the tropics are usually accompanied by enhanced convective activity[33]. Being an ocean-atmosphere coupled convective phenomenon, MJO activity is hence highly dependent on tropical SSTs, with higher MJO activity typically occurring when SSTs are higher[26]. Previous studies have shown accelerated warming over the Indo-Pacific warm pool and its expansion[11,34], which can potentially impact the MJO characteristics. To examine the changes in the warm pool, we estimate the surface area covered by the climatological 28°C isotherm of SST, during November–April (Figure 1), in the tropical Indo-Pacific region within 40°E–140°W, 25°S-25°N. Here we show that tropical SST warming has led to an almost twofold expansion of the Indo-Pacific warm pool, from an area of 2.2×10^7 km^2 during 1900–1980, to an area of 4×10^7 km^2 during 1981–2018 (Figure 1a, b, d). The warm pool expansion is non-uniform, with the SST warming more pronounced over the west Pacific in contrast to the Indian Ocean (Figure 1c). The difference in the warm pool expansion trends between the 1900–1980 and 1981–2018 periods is statistically significant at the 95% confidence levels. The shift in warm pool SSTs during the 1977–1980 period co-occur with the shift in global mean SSTs at the same time (Figure 1d), followed by an accelerated surface warming as a response to anthropogenic emissions[35]. It is important to note that the shift in SSTs also coincides with the positive phase of the Pacific Decadal Oscillation (PDO). A comparison of the warm pool area using multiple SST datasets shows that the changes in warm pool area presented here are robust (Extended Data Figure 3a). A breakpoint analysis confirms that the shifts to higher warm pool values occurred during 1979–1980 (Extended Data Figure 3b, c).

The changes in the MJO phase duration (Phases 5, 6 and 7) appears to be significantly correlated (Figure 3, Extended Data Figure 4) to the changes in SST collocated over the west Pacific warm pool, where the warming trends and the background mean SSTs are the largest. The fact that the correlation is significant even after the trends are removed suggests that the mechanisms working on the interannual and longer time scales are similar. SST warming is also large in the Indian Ocean, though it is interesting that these SST trends do not show any significant correlation with the MJO phase duration (Phases 5, 6 and 7). This might mean that the observed changes in the MJO phase duration is driven by SST changes in the west Pacific. In fact, an investigation of the atmospheric circulation shows enhanced convective activity and a strengthening of low-level westerlies over the west Pacific (120°E–160°E) associated with the trends in the MJO phase duration (Figure 3b). The enhanced convective activity over the west Pacific is compensated by subsidence over the central and west Indian Ocean (40°E–70°E). Pohl and Matthews[25] hypothesize that on interannual timescales when the west Pacific is warmer than normal, the latent heat release over the moist convective region decreases the effective static stability of the atmosphere and slows down the MJO over the warm pool. The long-term changes in the MJO phase duration and associated ocean-atmospheric interactions discerned here are consistent with the physical mechanisms observed for the MJO phase duration on interannual timescales[25,36].

MJO variability and propagation are largely linked to the moist static energy in the atmospheric column[36-38]. We inspected the specific humidity and temperature profiles independently, for a detailed examination of the factors driving the observed trends in the MJO phase duration (Figure 3c). While the MJO trends (Phases 5, 6 and 7) exhibit a positive correlation with the tropospheric temperatures over the warm pool from 90°E–170°E, the specific humidity anomalies show a significantly negative correlation over the Indian Ocean and positive correlation over the west Pacific. This indicates that while the warm SST trends in the west Pacific prolongs the local convective activity, it also drives dry air subsidence over the Indian Ocean (along with the moisture advected away from the basin), shortening the residence time of MJO over that region. Hence, though the entire Indo-Pacific SSTs are warming, it appears that the MJO response is more sensitive to the west Pacific SSTs—possibly because the SST trends and background mean values are relatively larger over this region during November–April. Meanwhile, the low-level winds associated with the observed changes in phase duration are westerly over the Indian Ocean (Figure 3b), converging into the west Pacific. This indicates that the prolonged residence time of MJO over the Maritime Continent may be supported by moisture supply from both local (west Pacific) and remote (Indian Ocean) sources. Extended Data Figure 5 shows a significant increase in tropospheric moisture (900–400 hPa levels) over the Maritime Continent-west Pacific warm pool region and a reduction in the moisture over the Indian Ocean. This is consistent with the previous studies[39] which suggest that the moisture gradient in the lower troposphere over the Indo-Pacific warm pool assist the eastward propagation of MJO.

A comparison of the MJO phase duration over the Maritime Continent and west Pacific warm pool area (120°E–160°E, 25°S–25°N, highlighted region in Figure 3, Phases 5, 6 and 7) demonstrates a considerable correlation (Pearson correlation, r=0.42; Kendall rank correlation, τ=0.3) statistically significant at the 95% confidence level (Figure 3d). The MJO phase duration over the Indian Ocean (Phase 1, 2 and 3) also shows a significant negative correlation with the west Pacific (r=-0.33), suggesting that the MJO changes over the Indian Ocean is also largely driven by SST warming over the west Pacific. A correlation with the trends removed from both the time series still shows statistical significance at the 90% confidence level, and it can be argued that the results of this analysis strongly hold, even if the large values of the correlation coefficient are due to the existence of a real trend. Meanwhile, the mean surface temperatures over the west Pacific also exhibit an interannual variability and long-term change similar to that of the warm pool expansion (Figure 3d, r=0.97, τ=0.86). The results presented here establish a clear role of warm pool expansion and increasing SSTs in shortening the residence time of MJO over the Indian Ocean by 3–4 days and prolonging it over the Maritime Continent by 5–6 days (Extended Data Figure 6). Such a large change in the MJO phase duration may have direct implications on the global weather and climate which is tightly linked to these MJO phases.

Impacts on global climate

To assess the potential impacts of the observed changes in the MJO phase duration on global climate, we performed a correlation analysis with the rainfall anomalies at each location across the globe, after removing the trends and ENSO-related variability. Figure 4a shows significantly large correlation between observed changes in the MJO phase duration and rainfall variability over the tropical and mid-latitude regions. The changes in the MJO phase duration over the Indo-Pacific are associated with enhanced rainfall over the Maritime Continent-west Pacific region, the Amazon basin in South America, southwest Africa and northern Australia (color shades in Figure 4a indicates correlation coefficients significant at the 95% confidence level). Meanwhile, the changes in MJO phase duration indicates a strong link with reduced rainfall over central and east Pacific, east Africa, Ganges basin in India, Yangtze basin in China and the east and west coasts of United States of America.

Interestingly, a trend analysis of rainfall for November–April shows consistent changes over some of these regions (Figure 4c). An increase in mean rainfall is observed over most of the Maritime Continent including southeast Asia (Indonesia, Philippines and Papua New Guinea), northern Australia, west Pacific, Amazon basin and southwest Africa. A decline in rainfall is observed over the central Pacific, Ecuador and along the west coast of United States (California). A slight decrease in rainfall is observed over the Yangtze basin in China and east coast of United States (Florida), consistent with changes in the MJO phase duration. The observed impacts are consistent with the MJO impacts on interannual timescales reported by previous studies[15], which means that similar processes are operating at interannual and lower frequency timescales (Extended

Data Figure 7). We confirm this with a composite analysis of the MJO events with longer phase duration for phase 5, 6 and 7 (standard deviation greater than one) which show similar results as in the correlation analysis and the trends (Figure 4b).

The recent California droughts (2013–2014, during which the MJO was in phases 5, 6 and 7 for 25–28 days), southeast Asia floods (in 2011, during which the MJO was in phases 5, 6 and 7 for 30 days) and east Africa droughts (2011) occurred during those years when the MJO phase duration was longer over the Maritime Continent and the west Pacific (Figure 2c). Extreme flooding events in Brazil, such as the 2011 Rio de Janeiro floods, have been linked to a strong MJO interacting with the South Atlantic Convergence Zone[10]. It cannot be ruled out that the same mean state change (namely warm pool expansion) can affect both the MJO and the regional rainfall changes presented here. In addition, large scale changes in the circulation due to Indo-Pacific warming[40] and the phase of the PDO could also interact with the MJO to influence the regional rainfall changes observed here. Regardless of their inter-relationship, we can certainly say that the Indo-Pacific warm pool expansion is not only changing the MJO but also these regional precipitation anomalies, either synergistically through the MJO or through independent pathways. Though we have not investigated the dynamics behind these events individually, we cannot overemphasize the need to closely monitor the changes in the Indo-Pacific warm pool for triggering or intensifying severe weather events in the future. Maintaining and enhancing existing ocean observational arrays over the Indian and Pacific basins and extending it to the straits in the southeast Asian maritime region is hence a high priority[41,42]. Climate model projections suggest further warming of the warm pool region, which may intensify the observed changes in MJO lifecycle in the future. However, state-of-the-art climate models fail to accurately simulate the observed distribution of SST changes over the Indo-Pacific even in the present climate, and hence may need further improvement (for example, via the subseasonal to seasonal prediction project[42,43]) in order to meet the challenges presented by a warming world. [4343]

References

1 McPhaden, M. J. Genesis and evolution of the 1997-98 El Niño. *Science* **283**, 950-954 (1999).

2 Maloney, E. D. & Hartmann, D. L. Modulation of eastern North Pacific hurricanes by the Madden–Julian oscillation. *Journal of climate* **13**, 1451-1460 (2000).

3 Klotzbach, P. J. & Oliver, E. C. Modulation of Atlantic basin tropical cyclone activity by the Madden–Julian oscillation (MJO) from 1905 to 2011. *Journal of Climate* **28**, 204-217 (2015).

4 Joseph, S., Sahai, A. & Goswami, B. Eastward propagating MJO during boreal summer and Indian monsoon droughts. *Climate Dynamics* **32**, 1139-1153 (2009).

5 Jia, X., Chen, L., Ren, F. & Li, C. Impacts of the MJO on winter rainfall and circulation in China. *Advances in Atmospheric Sciences* **28**, 521-533 (2011).

6 Wheeler, M. C., Hendon, H. H., Cleland, S., Meinke, H. & Donald, A. Impacts of the Madden–Julian oscillation on Australian rainfall and circulation. *Journal of Climate* **22**, 1482-1498 (2009).

7 Pohl, B. & Camberlin, P. Influence of the Madden–Julian oscillation on East African rainfall. I: Intraseasonal variability and regional dependency. *Quarterly Journal of the Royal Meteorological Society* **132**, 2521-2539 (2006).

8 Lorenz, D. J. & Hartmann, D. L. The effect of the MJO on the North American monsoon. *Journal of Climate* **19**, 333-343 (2006).

9 Grimm, A. M. Madden–Julian Oscillation impacts on South American summer monsoon season: precipitation anomalies, extreme events, teleconnections, and role in the MJO cycle. *Climate Dynamics*, 1-26 (2019).

10 Carvalho, L. M. V., Jones, C. & Liebmann, B. The South Atlantic convergence zone: Intensity, form, persistence, and relationships with intraseasonal to interannual activity and extreme rainfall. *Journal of Climate* **17**, 88-108 (2004).

11 Weller, E. *et al.* Human-caused Indo-Pacific warm pool expansion. *Science advances* **2**, e1501719 (2016).

12 Lazo, J. K., Lawson, M., Larsen, P. H. & Waldman, D. M. US economic sensitivity to weather variability. *Bulletin of the American Meteorological Society* **92**, 709-720 (2011).

13 Bertrand, J.-L. & Brusset, X. Managing the financial consequences of weather variability. *Journal of Asset Management* **19**, 301-315 (2018).

14 Kessler, W. S. EOF representations of the Madden–Julian oscillation and its connection with ENSO. *Journal of Climate* **14**, 3055-3061 (2001).

15 Zhang, C. Madden–Julian oscillation: Bridging weather and climate. *Bulletin of the American Meteorological Society* **94**, 1849-1870 (2013).

16 Cassou, C. Intraseasonal interaction between the Madden–Julian oscillation and the North Atlantic oscillation. *Nature* **455**, 523-527 (2008).

17 Stan, C. *et al.* Review of Tropical□Extratropical Teleconnections on Intraseasonal Time Scales. *Reviews of Geophysics* (2017).

18 Garfinkel, C. I., Feldstein, S. B., Waugh, D. W., Yoo, C. & Lee, S. Observed connection between stratospheric sudden warmings and the Madden□Julian Oscillation. *Geophysical Research Letters* **39** (2012).

19 Madden, R. A. & Julian, P. R. Observations of the 40-50-Day Tropical Oscillation - a Review. *Monthly Weather Review* **122**, 814-837 (1994).

20 Maloney, E. D., Adames, Á. F. & Bui, H. X. Madden–Julian oscillation changes under anthropogenic warming. *Nature Climate Change* **9**, 26 (2019).

21 Adames, Á. F., Kim, D., Sobel, A. H., Del Genio, A. & Wu, J. Changes in the structure and propagation of the MJO with increasing CO2. *Journal of Advances in Modeling Earth Systems* **9**, 1251-1268 (2017).

22 Oliver, E. C. & Thompson, K. R. A reconstruction of Madden–Julian Oscillation variability from 1905 to 2008. *Journal of Climate* **25**, 1996-2019 (2011).

23 Oliver, E. C. Blind use of reanalysis data: apparent trends in Madden–Julian Oscillation activity driven by observational changes. *International Journal of Climatology* **36**, 3458-3468 (2016).

24 Jones, C. & Carvalho, L. M. V. Changes in the activity of the Madden-Julian Oscillation during 1958-2004. *Journal of Climate* **19**, 6353-6370 (2006).

25 Pohl, B. & Matthews, A. J. Observed changes in the lifetime and amplitude of the Madden–Julian oscillation associated with interannual ENSO sea surface temperature anomalies. *Journal of Climate* **20**, 2659-2674 (2007).

26 Slingo, J. M., Rowell, D. P., Sperber, K. R. & Nortley, E. On the predictability of the interannual behaviour of the Madden-Julian Oscillation and its relationship with El Nino. *Quarterly Journal of the Royal Meteorological Society* **125**, 583-609 (1999).

27 Arnold, N. P., Kuang, Z. & Tziperman, E. Enhanced MJO-like variability at high SST. *Journal of Climate* **26**, 988-1001 (2013).

28 Zhang, C. & Ling, J. Barrier effect of the Indo-Pacific Maritime Continent on the MJO: Perspectives from tracking MJO precipitation. *Journal of Climate* **30**, 3439-3459 (2017).

29 Foltz, G. R. & McPhaden, M. J. The 30–70 day oscillations in the tropical Atlantic. *Geophysical research letters* **31** (2004).

30 Wheeler, M. C. & Hendon, H. H. An all-season real-time multivariate MJO index: Development of an index for monitoring and prediction. *Monthly Weather Review* **132**, 1917-1932 (2004).

31 Yoo, C., Feldstein, S. & Lee, S. The impact of the Madden□Julian Oscillation trend on the Arctic amplification of surface air temperature during the 1979–2008 boreal winter. *Geophysical Research Letters* **38** (2011).

32 Song, E. J. & Seo, K. H. Past□and present□day Madden□Julian Oscillation in CNRM□CM5. *Geophysical Research Letters* **43**, 4042-4048 (2016).

33 Roxy, M. Sensitivity of precipitation to sea surface temperature over the tropical summer monsoon region—and its quantification. *Climate Dynamics* **43**, 1159-1169, doi:10.1007/s00382-013-1881-y (2014).

34 Cravatte, S., Delcroix, T., Zhang, D., McPhaden, M. & Leloup, J. Observed freshening and warming of the western Pacific warm pool. *Climate Dynamics* **33**, 565-589 (2009).

35 Dong, L. & McPhaden, M. J. The role of external forcing and internal variability in regulating global mean surface temperatures on decadal timescales. *Environmental Research Letters* **12**, 034011 (2017).

36 Suematsu, T. & Miura, H. Zonal SST Difference as a Potential Environmental Factor Supporting the Longevity of the Madden–Julian Oscillation. *Journal of Climate* **31**, 7549-7564 (2018).

37 Sobel, A., Wang, S. & Kim, D. Moist static energy budget of the MJO during DYNAMO. *Journal of the Atmospheric Sciences* **71**, 4276-4291 (2014).

38 Kim, D., Kug, J.-S. & Sobel, A. H. Propagating versus nonpropagating Madden–Julian oscillation events. *Journal of Climate* **27**, 111-125 (2014).

39 Gonzalez, A. O. & Jiang, X. Winter mean lower tropospheric moisture over the Maritime Continent as a climate model diagnostic metric for the propagation of the Madden□Julian oscillation. *Geophysical Research Letters* **44**, 2588-2596 (2017).

40 Tokinaga, H., Xie, S.-P., Deser, C., Kosaka, Y. & Okumura, Y. M. Slowdown of the Walker circulation driven by tropical Indo-Pacific warming. *Nature* **491**, 439-443 (2012).

41 Hermes, J. C. *et al.* A sustained ocean observing system in the Indian Ocean for climate related scientific knowledge and societal needs. *Frontiers in Marine Science* **6**, 355 (2019).

42 Subramanian, A. *et al.* Ocean observations to improve our understanding, modeling, and forecasting of subseasonal-to-seasonal variability. *Frontiers in Marine Science* **6**, 427 (2019).

43 Vitart, F. & Robertson, A. W. The sub-seasonal to seasonal prediction project (S2S) and the prediction of extreme events. *npj Climate and Atmospheric Science* **1**, 3 (2018).

Acknowledgments

M.K.R. acknowledges NOAA/PMEL for the National Research Council Senior Research Associateship Award by the U.S. National Academy of Sciences (PMEL contribution no. 4975). P.D. was supported by the IITM Research Fellowship. D.K. was supported by the DOE RGMA program (DE□SC0016223), the NOAA CVP program (NA18OAR4310300), and the KMA R&D program (KMI2018-03110). We thank Nicholas Bond and Raghu Murtugudde for their comments on an early draft of this manuscript.

Author contributions

M.K.R. conceived the study, performed the analysis and prepared the manuscript. P.D. performed the MJO detection and initial analysis. T.S. provided additional MJO tracking algorithm for verification. All coauthors contributed to the interpretation of the results and drafting of the manuscript for publication.

Author information

Reprints and permissions information is available at www.nature.com/reprints. The authors declare no competing interests. Correspondence and requests for materials should be addressed to M.K.R.

Figure legends

Figure 1. A twofold expansion of the warm pool.

Indo-Pacific warm pool with its characteristic permanently warm SSTs of temperatures greater than 28°C for the period (**a**) 1900–1980 and (**b**) 1981–2018. The observed warm pool expansion is almost twofold, from an area of 2.2×10^7 km^2 during 1900–1980, to an area of 4×10^7 km^2 during 1981–2018. The warm pool area is estimated as the surface area covered by climatological 28°C isotherm of SST, during November–April, in the tropical Indo-Pacific region within 40°E–140°W, 25°S-25°N. (**c**) The observed trend in SST (°C per 37 years) during 1981-2018, for November–April. (**d**) Time series of the warm pool area during 1900–2018. Theil–Sen trend estimates are overlaid on the time series for the entire period (solid blue line, Sen slope of 2.25×10^5 km^2 per year) and for 1981–2018 (dashed blue line, Sen slope of 4.14×10^5 km^2 per year). The positive trend in warm pool area is significant at the 95% confidence level, according to the Mann–Kendall test. The grey shade overlaid on the time series represents ± two standard deviations of the warm pool area, based on monthly SST values. Yellow line represents global mean SSTs (°C) averaged for November–April. Warm pool SST values and area are based on HadISST dataset.

Figure 2. Changes in MJO lifecycle.

Time series (black line) and distribution of average yearly phase duration (in days) of MJO events during 1981–2018 over (**a**, **b**) the Indian Ocean (RMM phases 1, 2 and 3) and (**c**, **d**) the Maritime-west Pacific region (RMM phases 5, 6 and 7). Grey shading in (a, c) is ± two standard deviations of the MJO phase duration over a ten-year moving window. Pink lines overlaid on the time series represent the 20-year running trend of MJO phase duration (in days per year). Mann–Kendall test for the time series indicate that the trends are significant at the 95% confidence level. The phase duration distribution compares the probability density function of MJO phase duration during the earlier period (1981–1999) and later period (2000–2018), where $\mu 1$ and $\mu 2$ represents the mean number of days. $\mu 2$-$\mu 1$ indicates the change in MJO phase duration, with a decrease of 3–4 days over the Indian Ocean and increase of 5–6 days over the Maritime-west Pacific region. A Mann–Whitney test on the difference in the phase duration distributions in ***b***, ***d*** shows that the difference is statistically robust ($P < 0.05$), implying that the null hypothesis can be rejected.

Figure 3. Correlation between MJO phase duration and ocean-atmosphere conditions.

Correlation between MJO phase duration (phases 5, 6 and 7) with (**a**) SST anomalies, (**b**) winds and vertical velocity and (**c**) air temperature (colors) and specific humidity (contours) at each grid point over the Indo-Pacific basin for November–April, during 1981–2018 (n=37). The correlation analysis is performed after removing the trend and the ENSO variability from the time series. Color shading denotes correlation coefficients, with the significance at the 95% confidence levels noted below the color scale on top of ***a***. Vector arrow lengths are proportional to correlation coefficient according to the scale on top of ***b***. Thick contours in ***c*** denotes correlation coefficients significant at the 95% confidence level. The region within the solid black lines highlight the west Pacific warm pool region (120°E–160°E) where the ocean-atmospheric changes related to the MJO phase duration are the largest, and consistent across the various parameters. The longitude-pressure plots are averaged over 10°S–10°N. (**d**) Time series of MJO phase duration (phases 5, 6 and 7) and the surface area (km^2) enclosed by the 28°C isotherm of SST over the west Pacific (120°E–160°E, 25°S–25°N), during November–April, 1981–2018. Kendall rank correlation test (two tailed) for the two variables provided a tau coefficient of 0.3. The Kendall (τ) and Pearson (r) correlation coefficients shown are significant at the 95% confidence level (significant at the 90% confidence level after removing the trends, n=37). Yellow line overlaid on the time series represent the yearly mean SST over the west Pacific. Kendall rank correlation test for the west Pacific warm pool area and SST provided a tau coefficient of 0.86, significant at

95% confidence level.

Figure 4. Changes in global rainfall in response to the changes in MJO phase duration. (**a**) Correlation between the MJO (phases 5, 6 and) phase duration with rainfall anomalies for November–April, during 1981–2018. (**b**) Composite difference between years when MJO phase duration (phases 5, 6 and 7) is long and short (above and below 1 standard deviation). (**c**) Observed trend in rainfall (mm day^{-1} per 37 years) during the same period. The correlation and composite analyses are performed after removing the trend and the ENSO variability from the time series. Color shading denotes correlation coefficients and trends significant at the 95% confidence level. The circled regions indicate large continental areas where the trends in rainfall are consistent with the correlation and composite analyses. Red circles indicate increasing rainfall and blue circles indicate decreasing rainfall associated with the observed changes in MJO phase duration. Rainfall values are based on GPCP dataset.

Methods

MJO data and identification of events

The Real-time Multivariate MJO (RMM) index of Wheeler and Hendon[30], provided by the Australian Bureau of Meteorology, is used as a preliminary reference for identifying MJO events during 1981–2018. The RMM index[30] relies on an Empirical Orthogonal Function (EOF) analysis which combines equatorially averaged (15°S–15°N) lower (850 hPa) and upper (200 hPa) tropospheric zonal winds with outgoing longwave radiation (OLR, proxy indicator for convective activity). While the RMM index efficiently captures the dominant role of zonal winds during mature phases of strong MJO events, it can be inconsistent in representing the convective conditions associated with it[44-46]. As a result of this absence of interplay between circulation and convection, capturing the MJO events with its convective implications has been a conundrum—as the index occasionally captures non-existent events, while some events appear to occur early or late, or are even missing[28,44-47].

Hence, we identified MJO events by following a set of steps which consider the RMM index but clearly captures the MJO characteristics of eastward propagation and convective activity. We focus on the boreal autumn–winter–spring seasons (November–April) during which the MJO exhibits a prominent eastward propagation, and is sensitive to SST variations in the Indian and Pacific Ocean[48]. In order to factor in the convective activity, we used the daily OLR from the National Oceanic and Atmospheric Administration (NOAA) at 2.5° × 2.5° horizontal resolution, which has been conventionally used for detecting the MJO related convective activity. We also verified the detected events using the high resolution (1° × 1°) daily OLR Climate Data Record[49] (HIRS OLR), which is better suited for identifying the tropical variability at subseasonal timescales[50]. The MJO phase duration is strongly linked to the strength of MJO convection and its coupling with the largescale circulation[51]. Hence the current method makes sure to capture the MJO events which exhibit strong coupling between tropical convection and largescale circulation.

The OLR on subseasonal timescales also represents other types of equatorial propagating modes of convection, such as the westward moving equatorial Rossby waves, eastward moving Kelvin waves and mixed Rossby-gravity waves. The MJO component is hence filtered from the OLR data by including eastward zonal wavenumbers 1–5 and a period of 30–96 days, while the Kelvin wave component is separated by identifying eastward wavenumbers 1–14 and a period of 2–30 days, and equatorial Rossby waves by their westward zonal wavenumbers 1–10 and periods of 10–50 days[52,53]. We select eastward propagating convective MJO events in the filtered OLR anomalies, which are initiated in the Indian Ocean (Phases 1, 2 or 3)[28], proceed to the Pacific (Phases 6, 7 or 8) and propagate through at least six of the RMM phases with an average RMM amplitude greater than one (~1.5 standard deviation). We consider the initiation date as when the RMM index indicates MJO entry into the Indian Ocean from the west and starts to propagate eastward. We find 88 such MJO events over the 38 years, during November–April. The selected events are comparable to the MJO events detected by the tracking method used by Suematsu et al.[36], which is based solely on the RMM index at a threshold amplitude of 0.8, but with a relatively wide window for the band-pass filter (20–120 days).

Note that for computational purposes, the data for November–April is considered together as belonging to the initial year (e.g., MJO activity during November 1981–April 1982 is considered together as representing the year 1981). Hence, though we have 38 years of data, we consider it as 37 MJO seasons.

Warm pool SST and climate data analysis

HadISST1 SST data for the period 1900–2018, obtained from the Met Office Hadley Centre is used to estimate the changes in the Indo-Pacific warm pool and its role on the MJO phase duration. The warm pool area is estimated as the surface area covered by the climatological 28°C isotherm of SST, during November–April (Figure 1), in the tropical Indo-Pacific region within 40°E–140°W, 25°S-25°N. To examine the state and response of atmospheric circulation to the changing SSTs and MJO, we used air temperature, winds and specific humidity values for the tropospheric column from NCEP reanalysis for the period 1981–2018 at a 2.5° × 2.5° grid resolution. The global changes in rainfall are estimated using the NOAA GPCP Precipitation dataset which combines observations and satellite precipitation data on a 2.5° × 2.5° global grid.

A breakpoint analysis[54] is conducted to identify significant shifts in the mean of the Indo-Pacific warm pool time series (Extended Data Figure 3b). The analysis employs a Bai–Perron test[55] to determine the optimal number of breaks using Bayesian information criterion[56] and the residual sum of squares, given the minimum segment size of the time series (30-year segments used here). The location of these breakpoints can be attributed to the timing of non-linear changes in the observed warm pool area over time. The analysis was performed using the ‘strucchange’ package in the R Statistical Software[54].

The lifecycle of the MJO and the tropical ocean-atmosphere conditions are also dependent on the state of ENSO. We use a frequency bandpass filter (2–6 years) to remove the interannual frequency band associated with ENSO-related variations, though removing all of the ENSO related variability is difficult since it can influence variability at both higher and lower frequency. The correlation analysis and trends in Figure 3 and Figure 5 are estimated using these filtered anomalies. The least-square linear regression and Theil–Sen slope methods are used to estimate the observed trends. The Theil–Sen approach is considered more robust than the least-squares method due to its relative insensitivity to extreme values and better performance even for normally distributed data[57].

The statistical significance of the trends, correlations, and the difference of slopes[58] (Extended Data Figure 3c) is examined using standard two-tailed Student’s t-tests. The significance of the trends in the time series plots are further assessed with a Mann–Kendall test with block bootstrap to validate the significance when a time series shows auto-correlation[59]. Statistical significance exceeding the 95% confidence level is selected a priori as the level at which the null hypothesis can be rejected. The correlation analysis is also tested using Kendall rank correlation that is non-parametric and therefore makes no assumptions about the distribution and at the same time determine the direction and significance of the relation between the two variables[59]. The correlated variables are said to be concordant if their ranks vary together (+1) and discordant if they vary differently (-1). In order to compare the differences in the distribution of the MJO phase durations in Figure 2, we have used the Mann–Whitney test[60] to test the null hypothesis that there is no difference between two means (Extended Data Figure 8). The Mann-Whitney test is a non-parametric test useful for relatively short time series—and also takes into account the fact that MJO variability is not normally distributed about the mean state.

Methods References

44 Straub, K. H. MJO initiation in the real-time multivariate MJO index. *Journal of Climate* **26**, 1130-1151 (2013).

45 Liu, P. *et al.* A revised real-time multivariate MJO index. *Monthly Weather Review* **144**, 627-642 (2016).

46 Wolding, B. O. & Maloney, E. D. Objective diagnostics and the Madden–Julian oscillation. Part II: Application to moist static energy and moisture budgets. *Journal of Climate* **28**, 7786-7808 (2015).

47 Ventrice, M. J. *et al.* A modified multivariate Madden–Julian oscillation index using velocity potential. *Monthly Weather Review* **141**, 4197-4210 (2013).

48 Hendon, H. H., Wheeler, M. C. & Zhang, C. Seasonal dependence of the MJO–ENSO relationship. *Journal of Climate* **20**, 531-543 (2007).

49 Schreck, C., Lee, H.-T. & Knapp, K. HIRS Outgoing Longwave Radiation—Daily Climate Data Record: Application toward Identifying Tropical Subseasonal Variability. *Remote Sensing* **10**, 1325 (2018).

50 Kikuchi, K., Wang, B. & Kajikawa, Y. Bimodal representation of the tropical intraseasonal oscillation. *Climate Dynamics* **38**, 1989-2000 (2012).

51 Seo, K.-H. & Kumar, A. The onset and life span of the Madden–Julian oscillation. *Theoretical and Applied Climatology* **94**, 13-24 (2008).

52 Wheeler, M. & Kiladis, G. N. Convectively coupled equatorial waves: Analysis of clouds and temperature in the wavenumber–frequency domain. *Journal of the Atmospheric Sciences* **56**, 374-399 (1999).

53 Roundy, P. E., Schreck III, C. J. & Janiga, M. A. Contributions of convectively coupled equatorial Rossby waves and Kelvin waves to the real-time multivariate MJO indices. *Monthly Weather Review* **137**, 469-478 (2009).

54 Zeileis, A., Kleiber, C., Krämer, W. & Hornik, K. Testing and dating of structural changes in practice. *Computational Statistics & Data Analysis* **44**, 109-123 (2003).

55 Bai, J. & Perron, P. Computation and analysis of multiple structural change models. *Journal of applied econometrics* **18**, 1-22 (2003).

56 Schwarz, G. Estimating the dimension of a model. *The annals of statistics* **6**, 461-464 (1978).

57 Hirsch, R. M., Slack, J. R. & Smith, R. A. Techniques of trend analysis for monthly water quality data. *Water resources research* **18**, 107-121 (1982).

58 Cohen, P., West, S. G. & Aiken, L. S. *Applied multiple regression/correlation analysis for the behavioral sciences*. (Psychology Press, 2014).

59 Kendall, M. G. *Rank correlation methods*. 2 edn, (C. Griffin, 1948).

60 Mann, H. B. & Whitney, D. R. On a test of whether one of two random variables is stochastically larger than the other. *The annals of mathematical statistics*, 50-60 (1947).

Data availability

The MJO RMM index used in the study for the period 1981–2018 is available from the Australian Bureau of Meteorology (http://www.bom.gov.au/climate/mjo/). The monthly values of air temperature, specific humidity and winds, and the daily OLR and GPCP monthly precipitation can be obtained from the NOAA website (https://www.esrl.noaa.gov/psd/data/gridded/). HadISST data is available for download at the Met Office Hadley Centre website (https://www.metoffice.gov.uk/hadobs/hadisst/). The high resolution daily OLR data can be acquired from the University of Maryland OLR CDR portal (http://olr.umd.edu/).

Code availability

The MJO events identified in this study, and the code for estimating the individual MJO phase duration and the Indo-Pacific warm pool area, are available at https://github.com/RoxyKoll/warmpool-mjo. The code for filtering the MJO component from the OLR data is available from Carl Schreck at GitLab (https://k3.cicsnc.org/carl/carl-ncl-tools/blob/master/filter/filter_waves.ncl).

Extended data legends

Extended Data Figure 1. Typical lifecycle of MJO.

Composite anomalies of 30–100-day OLR (W m^{-2}) during November–April, for the period 1981–2018, showing the RMM Phases 1–8. Typically, the MJO events are initiated over the Indian Ocean and move eastward over the Maritime Continent to the Pacific (a–h). The region within the solid black lines highlight the west Pacific warm pool region (120°E–160°E) where ocean-atmospheric changes related to the MJO lifespan are the largest. OLR values are based on the NOAA interpolated OLR dataset.

Extended Data Figure 2. Annual average period of MJO events.

Time series of yearly average period of MJO events during November–April, 1981–2016 (Phases 1–8). The grey shade overlaid on the time series represents ±two standard deviations of the MJO phase duration over a ten-year moving window.

Extended Data Figure 3. Warm pool area in multiple datasets and breakpoint analysis.

(**a**) Time series of the warm pool area during November–April, 1900–2018, based on HadISST, ERSST_v3b and COBE_SST2 datasets. Theil–Sen trend estimates computed based on HadISST (as in Figure 1 of the main text) are overlaid on the time series for the entire period (solid blue line) and for 1981–2018 (dashed blue line). (**b**) Breakpoint analysis identifying the significant shifts in the mean of the Indo-Pacific warm pool time series, using HadISST. The breakpoint analysis shows two shifts in the time series, the first during 1945/46 and the second during 1979/80. Though the rate of change in warm pool area during 1900–1945 and 1946–1979 are different, the average warm pool area remains almost the same during both the periods. The breakpoint analysis confirms that the shifts to higher warm pool values occurred in the annual series during 1979–1980. (**c**) Table showing the trend in warm pool area using a range of breakpoints, from 1976/77 to 1982/83. The rate of warming does not change substantially with different breakpoints. At the same time, the difference between the trends are significant for all breakpoints considered. The significance of the difference between the slopes is estimated based on a t-test[58].

Extended Data Figure 4. Correlation between MJO phase duration and ocean-atmosphere conditions, without removing the trends.

Correlation between yearly average of MJO phase distribution (phases 5, 6 and 7) with (**a**) SST anomalies, (**b**) winds and vertical velocity and (**c**) air temperature (colors) and specific humidity (contours) over the Indo-Pacific basin for November–April, during 1981–2018 (n=37). The correlation analyses are performed after removing the ENSO variability from the time series, but without removing the trends.

Extended Data Figure 5. Trend in specific humidity anomalies.

Trend in specific humidity anomalies (g kg^{-1} 37 $years^{-1}$) for November–April, during 1981–2018. The trends indicate an increase (red colors) in tropospheric moisture over the warm pool region and a reduction (blue colors) in tropospheric moisture over the Indian Ocean (900-400 hPa levels).

Extended Data Figure 6. Schematic figure showing the changes in MJO lifecycle and impact on the global climate.

(a) As the Indo-Pacific warm pool expands with increasing sea surface temperatures, moist winds converge over the Maritime Continent-west Pacific, prolonging the MJO phase duration over this region by 5–6 days and shortening the MJO duration over the Indian Ocean by 3–4 days. (**b**) As a response to the changes in the MJO phase duration, an increase in mean rainfall is observed over most of the Maritime Continent including southeast Asia, and over northern Australia, west Pacific, Amazon basin and southwest Africa. A decline in rainfall is observed over the central Pacific, Ecuador and California, and a slight decrease in rainfall over the Yangtze basin in China and Florida.

Extended Data Figure 7. Relationship between MJO phase duration and global rainfall, without removing the trends.

Correlation between the MJO phase duration (phases 5, 6 and 7) with rainfall anomalies for November–April, during 1981–2018. The correlation analysis is performed after removing the ENSO variability from the time series, but without removing the trends. Rainfall values are based on GPCP dataset.

Extended Data Figure 8. Mann–Whitney test, for testing the significance of the differences in MJO phase duration.

The difference in the mean of MJO phase duration distributions are tested for different starting points. The P values are computed for different groups (1981–1999, 1982–1999 to 1990–1999) as the first sample and 2000–2018 as the second sample. (**a**) According to Mann–Whitney test, the difference in MJO phase duration (1,2,3) is statistically robust ($P < 0.05$, where we can reject the null hypothesis) for most part of the varying first sample (1981-1999 to 1990-1999, except 1987-1999 where $P = 0.07$). (**b**) For the MJO phase duration (5,6,7) the difference in mean is always statistically robust (where we can reject the null hypothesis) for the varying first sample (1981-1999 to 1990-1999, where P always < 0.05).

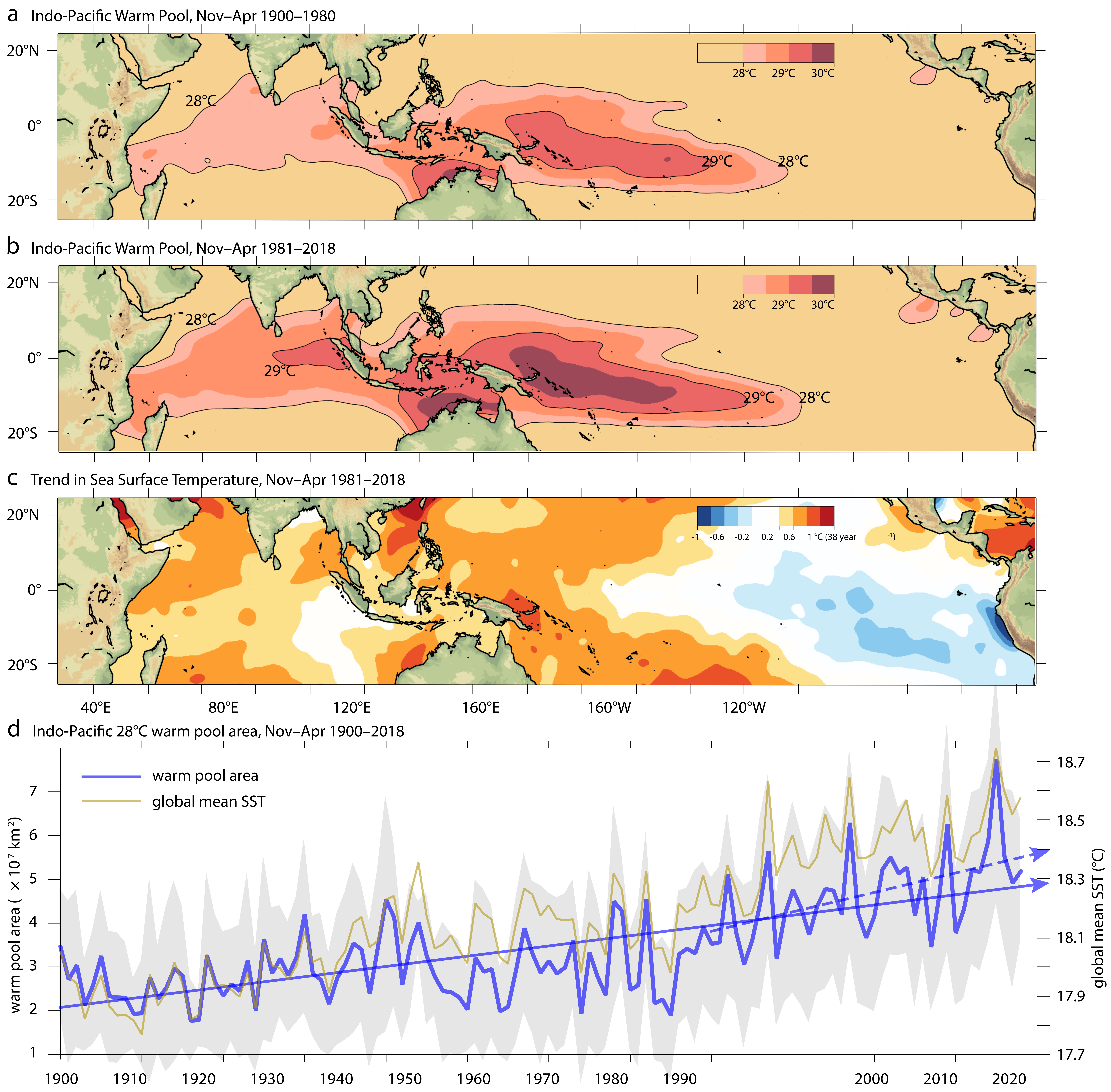
a Indo-Pacific Warm Pool, Nov–Apr 1900–1980
20°N
0°
20°S
28°C
29°C
30°C
28°C
29°C
28°C
b Indo-Pacific Warm Pool, Nov–Apr 1981–2018
20°N
0°
20°S
28°C
29°C
30°C
28°C
29°C
29°C
28°C
c Trend in Sea Surface Temperature, Nov–Apr 1981–2018
20°N
0°
20°S
-1 -0.6 -0.2 0.2 0.6 1 °C (38 year⁻¹)
40°E
80°E
120°E
160°E
160°W
120°W
d Indo-Pacific 28°C warm pool area, Nov–Apr 1900–2018
warm pool area
global mean SST
warm pool area (× 10⁷ km²)
global mean SST (°C)
1
2
3
4
5
6
7
17.7
17.9
18.1
18.3
18.5
18.7
1900
1910
1920
1930
1940
1950
1960
1970
1980
1990
2000
2010
2020

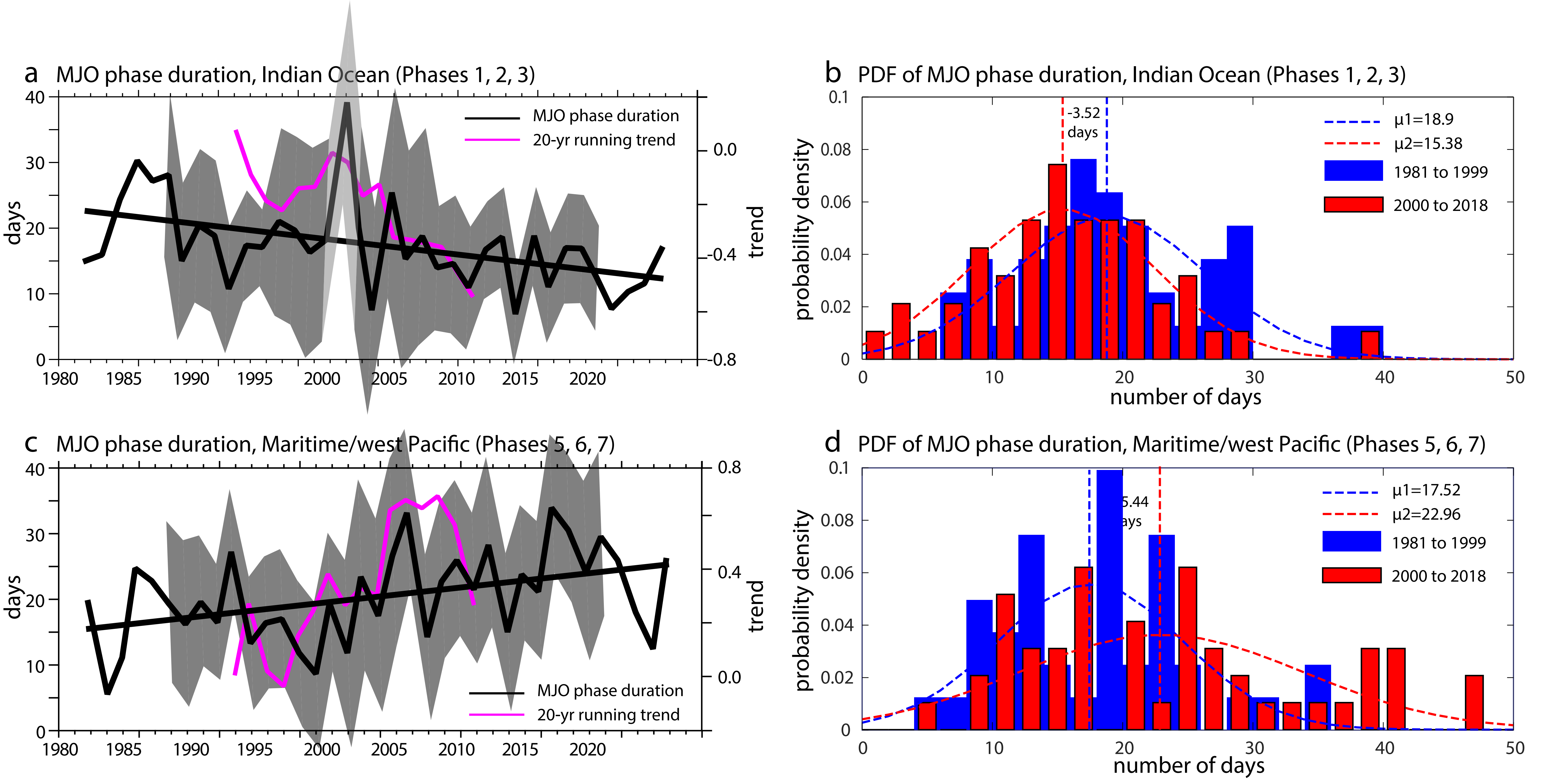

a MJO phase duration, Indian Ocean (Phases 1, 2, 3)
MJO phase duration
20-yr running trend
days
trend
b PDF of MJO phase duration, Indian Ocean (Phases 1, 2, 3)
-3.52 days
μ1=18.9
μ2=15.38
1981 to 1999
2000 to 2018
probability density
number of days
c MJO phase duration, Maritime/west Pacific (Phases 5, 6, 7)
MJO phase duration
20-yr running trend
days
trend
d PDF of MJO phase duration, Maritime/west Pacific (Phases 5, 6, 7)
μ1=17.52
μ2=22.96
1981 to 1999
2000 to 2018
probability density
number of days

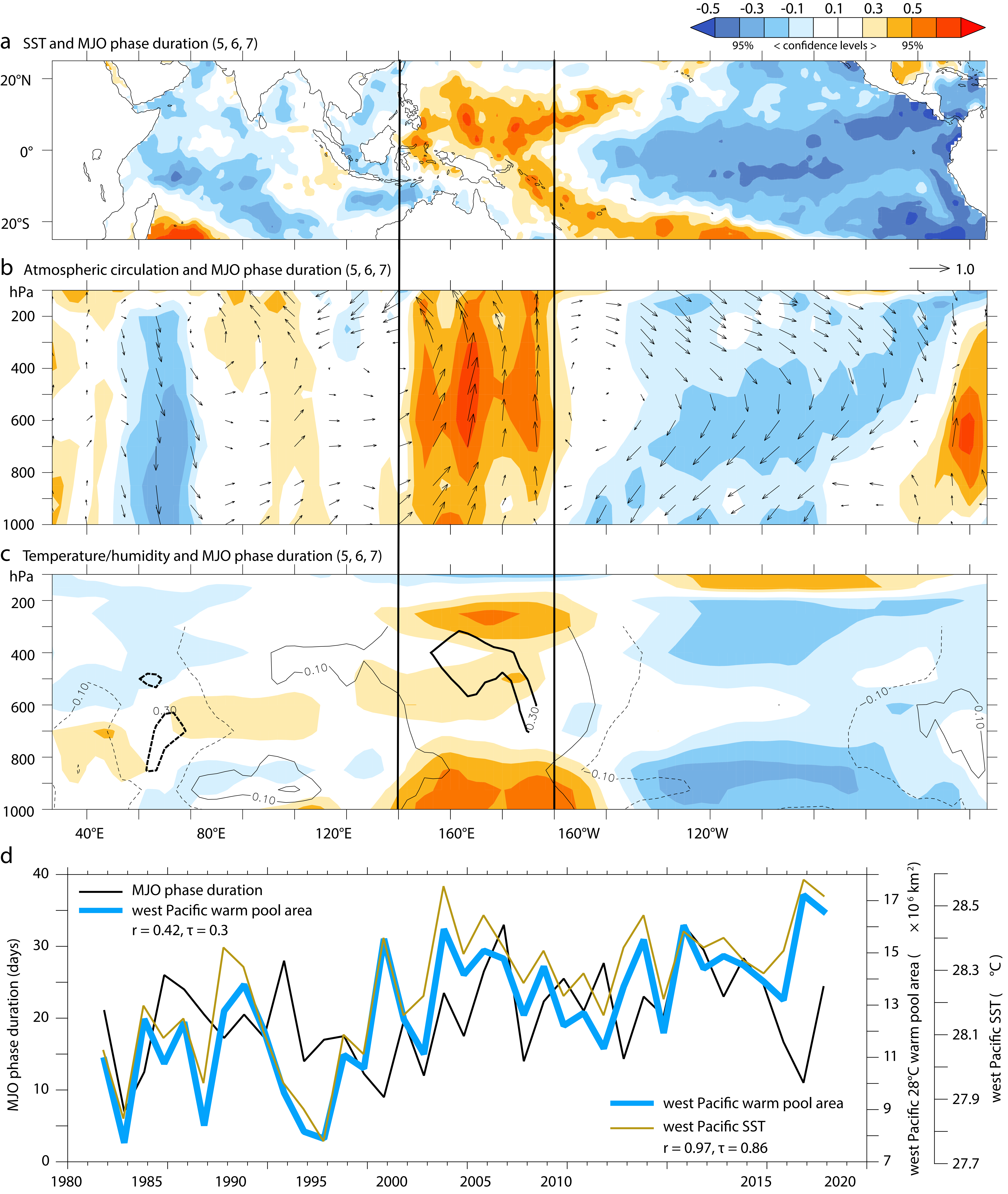

-0.5 -0.3 -0.1 0.1 0.3 0.5
95% < confidence levels > 95%
a SST and MJO phase duration (5, 6, 7)
20°N
0°
20°S
b Atmospheric circulation and MJO phase duration (5, 6, 7)
1.0
hPa
200
400
600
800
1000
c Temperature/humidity and MJO phase duration (5, 6, 7)
0.10
0.30
40°E
80°E
120°E
160°E
160°W
120°W
d
MJO phase duration
west Pacific warm pool area
r = 0.42, τ = 0.3
west Pacific warm pool area
west Pacific SST
r = 0.97, τ = 0.86
MJO phase duration (days)
west Pacific 28°C warm pool area (×10⁶ km²)
west Pacific SST (°C)
1980
1985
1990
1995
2000
2005
2010
2015
2020

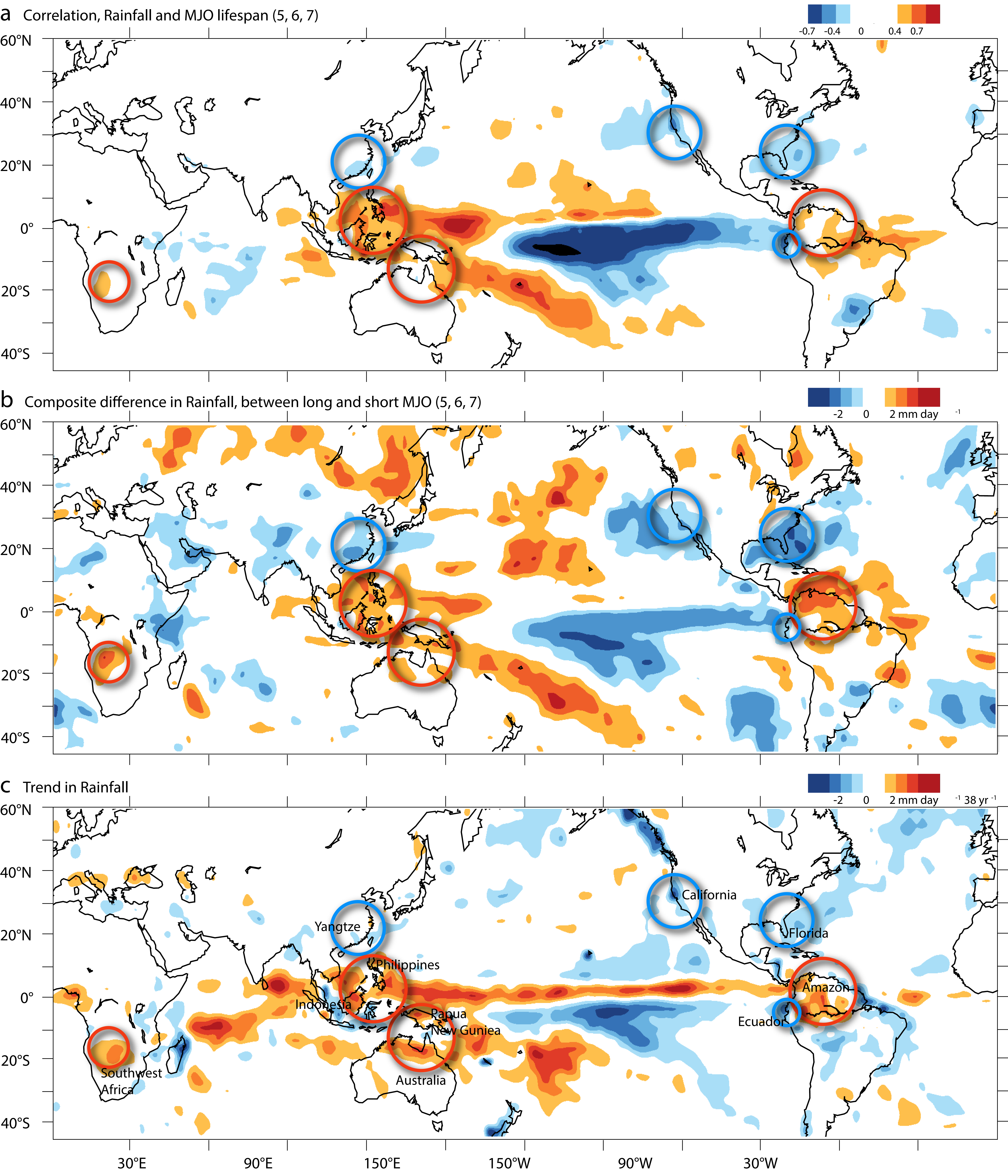

a Correlation, Rainfall and MJO lifespan (5, 6, 7)
-0.7 -0.4 0 0.4 0.7
b Composite difference in Rainfall, between long and short MJO (5, 6, 7)
-2 0 2 mm day -1
c Trend in Rainfall
-2 0 2 mm day -1 38 yr -1
60°N
40°N
20°N
0°
20°S
40°S
30°E
90°E
150°E
150°W
90°W
30°W
Yangtze
California
Florida
Philippines
Indonesia
Papua
New Guniea
Amazon
Ecuador
Southwest
Africa
Australia